PCCP

Accepted Manuscript

ROYAL SOCIETY OF CHEMISTRY

www.rsc.org/pccp

Complex interfaces in "phase-change" contrast agents

*Sabrina Capece[#], Fabio Domenici[#,§], Francesco Brasili[§], Letizia Oddo[#], Barbara Cerroni[#], Angelico Bedini[ç], Federico Bordi[§], Ester Chiessi[#] and Gaio Paradossi[#]**

[#]Dipartimento di Scienze e Tecnologie Chimiche, Università di Roma Tor Vergata, Via della Ricerca Scientifica 1, 00133 Rome, Italy. [§]Dipartimento di Fisica, Università di Roma Sapienza, P.le Aldo Moro 2, 00100 Rome, Italy. [ç]INAIL - Settore Ricerca Certificazione e Verifica - DITSIPIA. Via Fontana Candida, 1 Monteporzio Catone, 00040 Italy.

*E-mail paradossi@stc.uniroma2.it

Supplementary Information. Determination of CAC of DexMA in water. Interfacial tension determination measurements of the shell components. DSC determination of transition temperatures. MBs radial shrinking monitored by time lapse confocal microscopy experiments. Fluorescence microscopy during US irradiation. Example of simulation of the time evolution of the radial shrinking with fixed shear viscosity. References.

ABSTRACT

In this paper we report on the study of the interface of hybrid shell droplets encapsulating decafluoropentane (DFP), which exhibit interesting potentialities for ultrasound (US) imaging. The fabrication of the droplet is based on the deposition of a dextran methacrylate layer onto the surface of surfactants. The droplets have been stabilized against coalescence by UV curing, introducing crosslinks in the polymer layer and transforming the shell into an elastomeric membrane with a thickness of about 200 nm with viscoelastic behaviour. US irradiation induces the evaporation of the DFP core of the droplets transforming the particles into microbubbles. The presence of a robust crosslinked polymer shell introduces an unusual stability of the droplets also during the core phase transition and allows recovering of the initial droplets state after few minutes from switching off US. The interfacial tension of the droplets has been investigated with two approaches, the pendant drop method and an indirect method, based on the determination of the liquid ↔ gas transition point of DFP confined in the droplets core. The re-condensation process has been followed by capturing images of single MBs by confocal microscopy. The time evolution of microbubbles relaxation to droplets was analysed in terms of a modified Church model to account for the structural complexity of the MBs shell, i.e. a crosslinked polymer layer over a layer of surfactants. In this way the microrheology parameters of the shell were determined. In a previous paper (*Chem. Commun.*, 2013, **49**, 5763 - 5765) we showed that these systems could be used as UCAs. In this work we substantiate this view assessing some key features offered by the viscoelastic nature of the droplet shell.

INTRODUCTION

Many research topics address the realm of "nano" to find new properties and functionalities. However, this tendency toward the extreme miniaturization finds a limit when dealing with ultrasoun contrast agents (UCAs). In clinical sonography, UCAs size is dictated by the working frequency of the operating medical US scanners and it should be in the range of a few microns in order to produce an efficient scattering of the US waves.[1] Since the first observations of the enhancement of US echoes induced by the intravenous injection of air microbubbles (MBs) in saline, several types of MBs have been developed with the goal to increase the US backscattering efficiency. Recently, MBs have also been proposed as multimodal contrast agents, with the ability to transport and deliver upon irradiation a drug cargo, thus approaching the concept of theranostic device.[2]

The design of theranostic MBs implies to master the surface and interface properties of microsystems.[3] For this reason new approaches in MBs fabrication have been applied using microfluidics,[4-8] inkjet technology,[9,10] and high shear stirring methods.[11] At the present, two main classes of MBs, lipid or polymeric, are available on the market. The attention of many researchers addressed lipid shells containing hydrophobic gases such as sulphur hexafluoride (SF_6), or perfluorocarbons (PFCs). The use of such gasses extends the half-life of lipid MBs from seconds to minutes.[12] In addition, these gasses, bearing magnetically active nuclei of ^{19}F, offer the possibility to support multimodal imaging from sonography to magnetic resonance imaging (MRI).[13] Polymer shelled MBs are more stable than the lipid ones, with a circulation life of many hours although this advantage is generally paid with a lower ability to scatter US due to a thicker shell.[14] Sometime this disadvantage is reduced as in the case of poly (vinyl alcohol) (PVA) shelled MBs compared to the pure lipid ones marketed as SonoVue®.[15] Moreover, polymer shelled MBs offer versatile surfaces, keen to modification by tethering ligands to target receptors of cancer cells, poly (ethylene glycol) chains to increase the stealth effect, drug cargos or active molecules for multimodal imaging.[16] All

these features favour the active targeting of pathological tissues, implementing the diagnostic capabilities of MBs.[17]

PFCs can be found in standard conditions both in the gas or liquid state, depending on their molecular weight. Recently, they have been used not only to stabilize lipid or polymer shelled MBs, but also as component of the liquid core of lipid or polymer shelled droplets dispersed in an aqueous medium.[18] Interestingly, the core of such systems can undergo a liquid ↔ gas transition, and US can be used to trigger the phase transition, transforming the droplet into an MB with echogenic properties.[19,20] In this case the transition is termed acoustic droplet vaporization (ADV) and is at the base of the "phase-change" contrast agents properties.[21] This transition depends both on the thermodynamic properties of the liquid core, as the boiling point and the enthalpy of evaporation, and on the shell properties such as the radius, r, and the surface tension, σ. In particular the surface tension of the shell offers an additional pressure, $P_{IN,}$ over the external pressure, $P_{0,}$ which is described by the Laplace equation for the simple liquid/gas spherical interface.[22]

$$\Delta P = P_{IN} - P_0 = \frac{2\sigma}{r} \qquad (1)$$

According to this equation, for a water/PFC interface the pressure of PFC vapour in the droplet core at the boiling point will increase correspondingly by an extra pressure, P_{IN}. Due to the presence of a size distribution, not all the droplets will be activated simultaneously. "Phase-change" droplets have been studied for their potentials in drug release. It has been reported that the efficiency for drugs or genes release of hard-shelled MBs[23] is comparable or better than liposomes,[24] polymer micelles,[25,26] capsules[27] or emulsions[28] when they are triggered by inertial cavitation.

During the phase transition, a shell can break or resist to the pressure build-up. Clearly, for imaging purposes the resistance of the shell to the liquid vapour transition of the core is a relevant issue. Recently, a study on lipid droplets encapsulating superheated perfluoropropane and perfluorobutane, highlighted the importance of the lipid composition in the stabilization and activation energy of vaporization/condensation phase change induced by heating metastable

nanodroplets or by pressurizing lipid MBs encapsulating perfluorobutane.[29,30] ADV has been studied with O/W emulsions,[31] surfactants stabilized miniemulsions and amphiphillic polymers.[32] The approach described in this paper aims to increase the life and resilience of the phase-change droplets by photo-polymerizing the methacrylate moiety grafted on the biopolymer chains in order to have a viscoelastic shell able to stretch during the core evaporation triggered by US and to recover the previous size once the DFP core is re-condensed. In this respect, we present a study of the properties of MBs with a hybrid shell where an amphiphilic biodegradable polymer, dextran methacryate (DexMA) layer is deposited on top of a monolayer of surfactants encapsulating a decafluoropentane (DFP) liquid core. In normal conditions, i.e. at room temperature and 1 atm, DFP has a boiling point T_b= 56 °C, well above physiological temperature.

Recently it has been reported that the ADV effect is mainly due to two phenomena, a highly non linear distortion of the acoustic wave and the focusing of the distorted wave within the droplet, explaining why to accomplish ADV with droplets of a few microns a high pressure threshold is not necessary.[33] In the droplet sketched in Scheme 1, the crosslinked polymer chains are responsible for the elastomeric behaviour of the shell. Upon US pressure field, the DFP core undergoes ADV and the chemically crosslinked polymer component provides an elastic retraction force, which makes the behaviour of these MBs very different in comparison to one-component lipid or uncrosslinked polymer shelled ones. In particular, the ADV process can be cycled *via* a series of evaporation – condensation steps driven by a "switch on – switch off" US duty sequence. These new features could provide a more versatile contrast enhancement agent for US imaging[11].

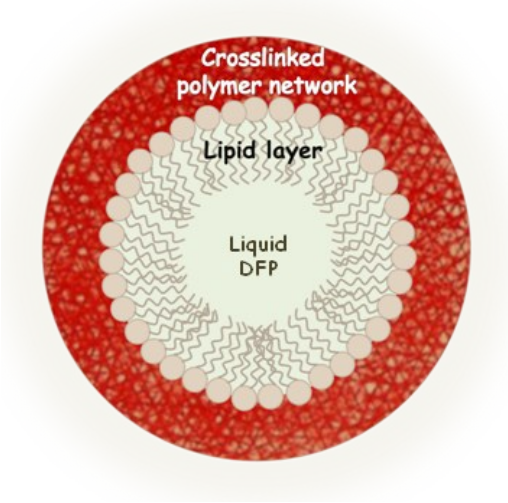

Scheme 1. A DFP encapsulated droplet with lipid/crosslinked polymer hybrid shell.

EXPERIMENTAL SECTION

Materials

Dextran (Dex) *from Leuconostoc mesenteroides* M_w 35000-40000, palmitic acid (PA) 1,1,1,2,3,4,4,5,5,5-decafluoropentane (DFP) with T_b= 56 °C, pyrene, rhodamine B isothyocyanate-mixed isomers (RBITC), fluoresceine isothyocyanate (FITC), nile red and acetone were Sigma-Aldrich products (Milan, Italy). Epikuron®200 was purchased from Cargill Texturizing Solutions GmbH & Co. (Hamburg, Germany). 2-Hydroxy-1-[4-(2-hydroxyethoxy)phenyl]-2-methyl-1-propanone, IRGACURE® 2959, was from BASF (Kaisten, Switzerland). Chloroform was from Carlo Erba Reagents (Milan, Italy). Ultrapure water (18.2 MΩ·cm) was produced by a deionization apparatus PureLab (USF, Perugia, Italy).

Preparation and characterization of micro and nano-droplets

DexMA shelled microdroplets were prepared according to the method previously described in literature.[11] A detailed description is provided in the Electronic Supplementary Information (ESI). A modification of this method was used to prepare DexMA shelled nanodroplets. In brief, after dispersing all the components in water, the mixture was subjected to a pre-homogenization step with an UltraTurrax T25 at 15000 rpm for 5 minutes. An US probe operating at 20 KHz, Vibra-Cell VCX 400, Sonics & Materials, Inc. (Danbury, Connecticut, USA) was then placed into the sample, immersed in an ice bath, and switched on for 3 minutes with a 50 % of the maximum amplitude pulse. The mixture was then cured by UV exposure as described above for 20 minutes and left overnight to react. The high density of DFP caused the particles to settle down so the washing was performed by suspending in water the pellet obtained after 20 minutes of centrifugation at 3000 rpm. Particles concentration was determined by using a Neubauer chamber with a 40x objective (Plan Fluor, Nikon, Florence, Italy). Micro or nanodroplets mean diameter values and size distribution were assessed with confocal microscopy or dynamic light scattering, respectively. RBITC-labeled droplets were prepared by adding 4 μL of a stock solution of RBITC (2 mg/mL in

anhydrous DMSO) per mL of sample, leaving the mixture to react under slow stirring in the dark for 2 hours. The excess dye was washed as supernatant after centrifugation for 4 minutes at 1000 rpm. Particles collected as a pellet were usually re-suspended in water. DexMA microdroplet prepared with this procedure remain stable also after 5 "switch on – switch off" US duty cycles.

DexMA droplets containing nile red in the DFP core were prepared by dissolving the solvatochromic dye in the oil phase, i.e. DFP, at a concentration of 60 μg/mL.

Thermogravimetric (TGA) and Differential Thermal Analysis (DTA)

TGA and DTA were performed using an SDT Q600, TA-Instruments Inc. (Milan, Italy) on freeze-dried DexMA microdroplets, typically obtaining 18 mg of powder from 11.4 mL of aqueous suspension. About 2 mg of the lyophilized sample was weighed in an alumina pan, placed in the TGA furnace and heated from 50 to 1000 °C at a rate of 10 °C/min under nitrogen purge (flow rate 100 mL/min). Both weight loss as a function of temperature and DTA curves were recorded. An empty pan was used as reference.

Surface tension and interfacial tension measurements

Surface and interfacial tension measurements were performed by the pendant drop method using a Theta Lite AtTension Optical Tensiometer from Biolin Scientific Oy. (Espoo, Finland). The measurements were carried out at the laboratories of Biolin Scientific, Espoo, Finland, under the supervision of Dr. Susanna Laurén. Details of the measurements are given in the Supplementary Information.

Differential Scanning Calorimetry (DSC)

DSC measurements were performed by using a Q-200 scanning calorimeter, TA-Instruments Inc. (Milan, Italy), equipped with a refrigerated cooling system RCS-90, TA-Instruments Inc. (Milan, Italy), using aluminum pans, Tzero® Pans, with Tzero® hermetic lids with a Tzero® sample Press Kit, TA-Instruments Inc. (Milan, Italy). Samples of 20 mg of microdroplets prepared according to the method described in ESI, were analyzed in the absence and in the presence of the photoinitiator

Irgacure®2959 in order to trigger the shell crosslinking after 20 min of UV curing. An empty pan was used as reference. Thermograms were recorded under nitrogen atmosphere with a flow rate of 50 mL/min, at 1 °C/min after 1 min of equilibration at the starting temperature of 10 °C. Intermediate components mixtures were explored as well and are reported in Supplementary Information.

Acoustic Droplet Vaporization (ADV)

SP100 sonoporator, Sonidel (Dublin, Ireland) was used to prove the droplet ↔ bubble transition upon US application. US were applied continuously, duty cycle 100%, at a central frequency of 1 MHz, for 30 seconds, with a nominal intensity of 3.6 $W \cdot cm^{-2}$, a transducer with an effective radiating area of 0.8 cm^2 emitting unfocussed US. The droplets, $3 \cdot 10^8$ MBs suspended in 3 cm^3 of water, were placed in a plastic vial with a section of 1 cm^2 and a height of 10 cm. The acoustic contact was assured by placing ca. 5 cm^3 of gel for medical sonography, PBpharma (Turin, Italy), between the probe and the bottom of the vial. The acoustic fields produced by the US source was characterized as a 1 MHz sinusoidal wave. We measured the acoustic pressure by means of a needle hydrophone S.N. 1470, Precision Acoustics, (Bockhampton, England) of 1 mm diameter with sensitivity of 1670.4 mV/MPa (± 14%), at varying the distance from the source, located below the sample holder. The intensity of the acoustic field was thus expressed in terms of Spatial Peak Temporal Peak (SPTP) intensity, (the higher measured value), which is significantly correlated with mechanical bioeffects induced by US.[34] The (SPTP) intensity, averaged along the sample holder depth, resulted 3 ± 1 W/cm^2. According to the determined acoustic parameters, the mechanical index, was estimated to be 0.3. The apparently low

Widefield Fluorescence and Confocal Laser Scanning Microscopy (CLSM)

A Nikon Eclipse Ti microscope with a Plan Apo 60× oil immersion objectives, Nikon (Florence, Italy) equipped with Ar^+, Spectra Physics, (Mountain View, California), and He-Ne, Melles Griot (Florence, Italy) lasers and a sCMOS Andor Zyla 4.2 camera, Andor Instruments (Belfast, Northen

Ireland) was used in this work. Description of the set-up and of the experimental procedure is given in the electronic supplementary information (ESI).

Dynamic Light Scattering (DLS)

The average hydrodynamic diameter of nanodroplets was evaluated at room temperature using a BI-200SM goniometer, Brookhaven Instruments Co, equipped with a laser source at 532 nm and a BI-9000AT correlation board. Temperature was controlled with an external thermostat circulating water in a coil placed in the vat containing the refractive index matching liquid. Analysis of the autocorrelation function, g^2 (q, t), of the scattered intensity was carried out using the CONTIN algorithm of the standard software package of the instrument.

Numerical integration of the Church and modified Church equations

The numerical solutions of the nonlinear equations describing the relaxation dynamics of the MBs were performed using the software Wolfram Mathematica V10.1. The optimized solutions were obtained using the Levenberg-Marquardt χ^2 minimization algorithm. The goodness of the parameters of each fit was evaluated in terms of the reduced χ^2 of the nonlinear solutions.

Atomic force microscopy (AFM)

AFM was performed on microdroplets physisorbed via electrostatic interaction onto aminosilane-coated silicon wafers, Ted Pella (Milan, Italy). Tapping-mode AFM topography was performed by using a Dimension ICON microscope equipped with Nanoscope V Controller, Bruker AXS, (Germany). AFM images were acquired in air at room temperature, using a cantilever force constant of 40 N/m, a scan rate of 0.3 Hz, and different scan sizes (512×512 pixel resolution).

RESULTS AND DISCUSSION

Characterization of the droplets and ADV behaviour

Recently we described a general strategy for obtaining crosslinked polymer shelled, biodegradable microdroplets with DFP liquid core, which can be vaporized by US application.[11] The method can be adapted to obtain instead nanodroplets, with an average size of 700 nanometers, as showed in Figure 1, a and b.

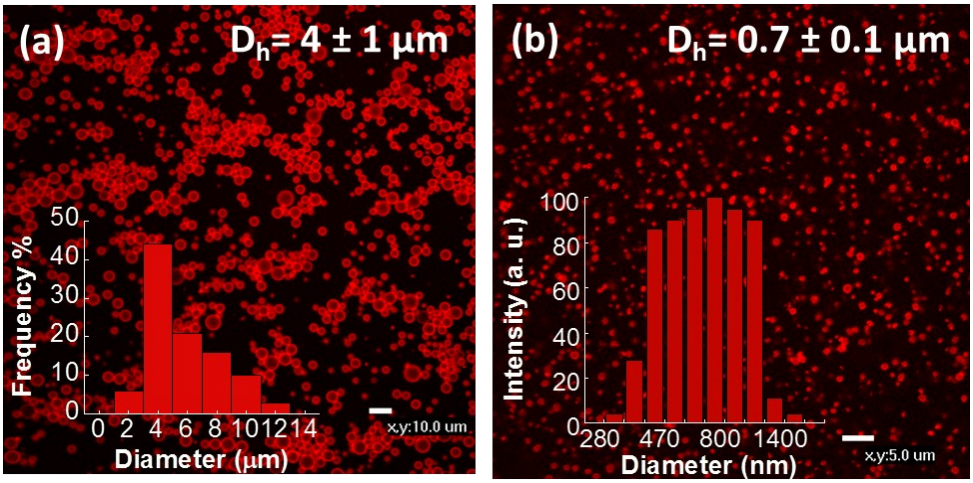

Figure 1. CLSM of (a) RBITC-labeled samples of DexMA shelled microdroplets and (b) DexMA shelled nanodroplets at 60× and 100× magnification, respectively. Insets: size distributions and average diameters values. DexMA shelled microdroplets and nanodroplets size distributions were determined by CLSM and DLS, respectively.

The reduction of droplets size can be accomplished by an additional energy input during the components dispersion, before the UV curing, by exposing the mixture to high power US irradiation at a frequency of 20 kHz. The role of the crosslinks in stabilizing the microdroplets clearly emerges when size and number of particles with and without UV curing are compared. The average diameter and number density of UV cured, i.e. crosslinked, DexMA microdroplets as a function of time is shown in Figure 2a and compared with the same quantities for uncured droplets, shown in Figure 2b. Initially the average diameters of the uncrosslinked and of the UV cured DexMA droplets are almost the same. However, after two days a three-fold average increase of the uncrosslinked droplets diameter is observed, with a consequent drop of the uncrosslinked droplets number, due to

a typical coalescence process. The presence of the polymer at the surface of the surfactants layer do not hinder this process, since the chains are able to move and redistribute all over the shell.[35]

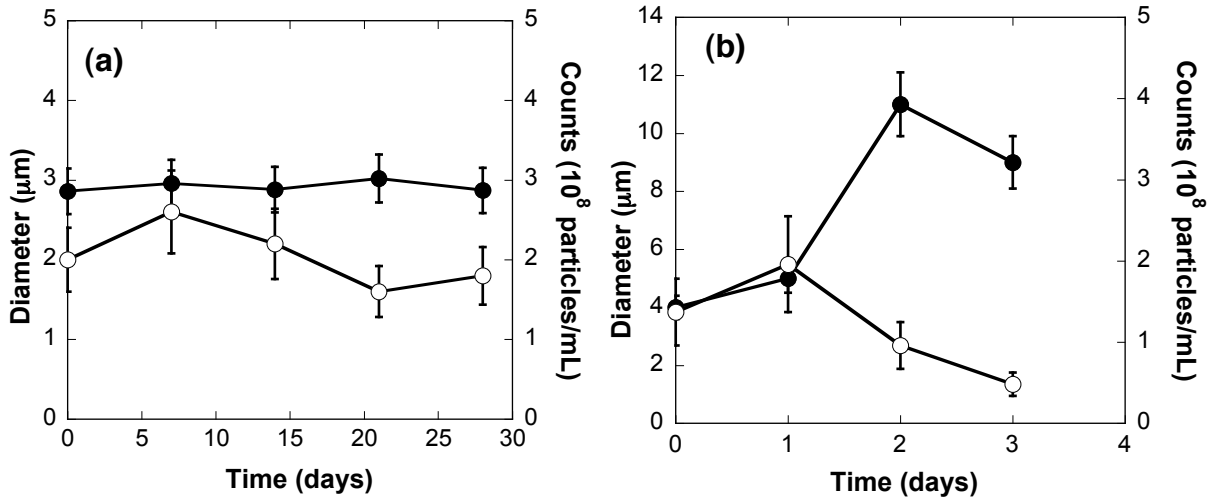

Figure 2.Mean diameter (●) and counts (○) as a function of time for UV (a) cured and (b) not cured DexMA microdroplets. Concentrations of surfactants and DexMA are the same in both cases.

The amount of polymer deposited on the lipid shell after UV curing can be estimated by thermogravimetric analysis (TGA), see Figure 3. Lipids and unmodified dextran are reported to decompose at 180–250 and at 230–400 °C, respectively, with a partial overlap of the two process.[36, 37] Then, assuming that the surfactants are totally distributed at the DFP/water interface, it is possible from the TGA thermograms to assess the relative composition of the microdroplet shells: DexMA: surfactants: pyrolysis residues as 71:14:15. The mass of DexMA, determined by TGA, corresponds to a concentration of 1 mg/mL in solution, in good agreement with the critical aggregation concentration (CAC) of the polymer determined by the pyrene method (see Figure S1a and S1b of ESI).

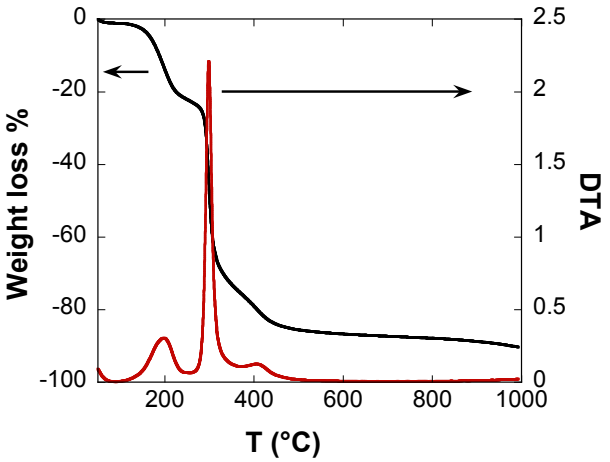

Figure 3. TGA (black line) and DTA (red line) thermograms of freeze-dried DexMA shelled microdroplets. Endothermic heat: up.

These hybrid droplets, encapsulating liquid DFP, undergo a liquid ↔ gas phase transition,[11] when a 1 MHz US wave exerts a negative pressure of about 0.3 MPa (SPTP intensity) at the conditions specified on the experimental part. The transition is evidenced by the floating of the particles at the meniscus of the dispersing liquid (water), once US are activated. Differently from the microdroplets, nanodroplets, upon identical US irradiation conditions, do not display such a transition. This is probably due to an higher Laplace contribution to P_{IN} (eq 1) coming from the higher curvature of the droplet shell. The interfacial tension is a key parameter in "phase-change" system undergoing a liquid ↔ gas transition as in ADV. We approached the knowledge of this parameter by analysing the single components of the hybrid microdroplets and the overall shell interfaces with water using the direct method of the pendant drop (see Figure S2 of ESI) and an indirect method exploiting the results collected by DSC. A summary of the interfacial tensions obtained by the pendant drop method with different components of our core/shell surfaces is shown in Table 1 of ESI.

These findings confirm the amphiphilic behaviour of DexMA in the uncrosslinked state as the surface tension of the droplet interface is decreased of about 5 mN/m upon the addition of polymer at a concentration of 0.1 % (w/V). By increasing the polymer concentration to 1 % (w/V) the interfacial droplets tension does not change within the experimental errors, providing an indirect validation of the CAC obtained by means of the pyrene method described in ESI.

The UV curing transforms the polymer layer into a polymer elastomer, leading to an increase of the surface tension of the droplet. The curing poses some experimental limitations to the application of the pendant drop method as the photopolymerization process triggered by the UV light makes the dispersing phase opaque to the recording system of the instrumentation. For this reason the surface tension study was limited to the early stages of the annealing step after the photopolymerization. The value reported in Table 1, Test F, is taken ten minutes after irradiation whereas in droplets fabrication the annealing duration was prolonged overnight. With higher polymer concentration, Test G of Table 1, the interfacial tension is assessed by inverting the phases (Figure S2b of ESI), with DFP surrounding the water as drop phase. In this modality the buoyancy of the water drop is assured by the higher density of DFP.

To assess the interfacial tension of the droplet shell, we measured the liquid ↔ gas transition points of different interphases by DSC, from the simple DFP/water up to the complex DFP/Epikuron-PA/DEXMA/water with and without UV curing. The results are summarized in Table 2 of ESI

DSC thermograms of UV cured and uncured DexMA, C=1 % (w/V), shelled microdroplets are reported in Figure 4, showing a dramatic change in the DSC behaviour. Before curing, the DSC thermogram displays a single sharp peak relative to the DFP evaporation at 77.4 °C (Figure 4a), Test 8 of Table 2 of ESI, displaced of about 20 °C with respect to the transition point in standard condition (see in ESI, Figure S3a). The effect of the UV curing changes dramatically the DSC behaviour of the droplet. The DSC profile of the shell with crosslinked polymer chains (Figure 4b) is similar to the thermograms reported for the melting process occurring in solid nanoparticles.[38,39]

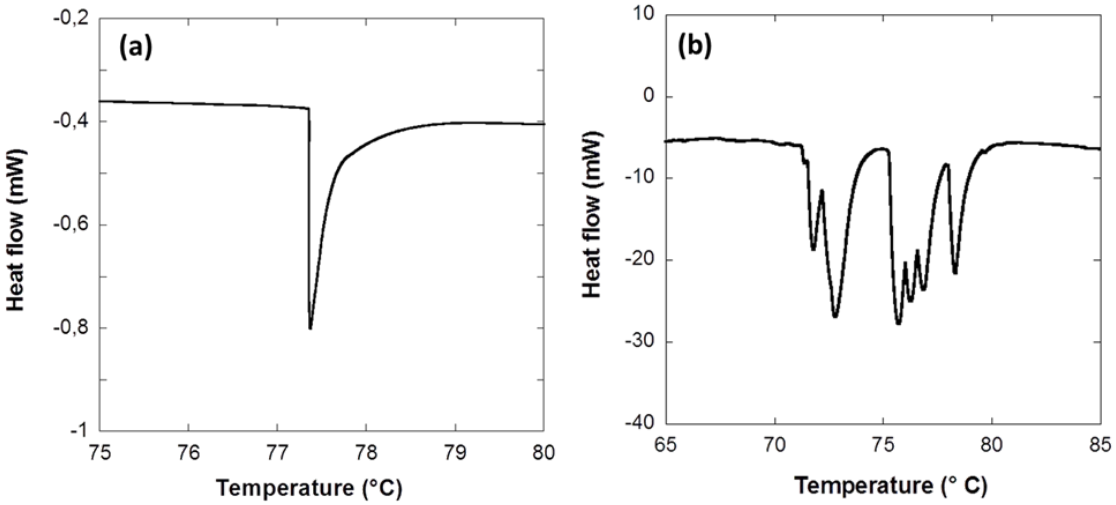

Figure 4. DSC thermogram of (a) uncrosslinked and (b) crosslinked DexMA droplets. Exothermic heat: up

The thermogram complexity, showing several peaks in the range of temperatures from 72 to 78 °C, is related to the size distribution of the microdroplets, (inset of Figure 1a), as well as to the structural heterogeneities introduced by the UV curing process. The size distribution affects the transition because of the "Laplace pressure" term that adds up to the standard pressure, which depends on the size of the droplet, (eq 1).

DSC data can be used to estimate the interfacial tension of the droplets with fully crosslinked polymer shell, whereas the pendant drop method previously illustrated, is restricted to the initial stage of the curing process. For a curved surface with radius r the overall tension can be estimated according to:

$$\sigma = \frac{rP_0}{2}\left\{exp\left[-\frac{\Delta H_v}{R}\left(\frac{1}{T}-\frac{1}{T_0}\right)\right]-1\right\} \qquad (2)$$

where ΔH_v, the evaporation enthalpy of the DFP core, 21.2 kJ·mol^{-1}, is assumed independent from pressure and temperature, T and T_0 are the transition temperatures of DPF in the droplet and in a flat DFP/water interface, respectively, determined via DSC and R is the gas constant. Eq 2 can be compared with eq 21 obtained by Evans.[40] In this analysis the value of the interfacial tension, σ, is calculated as the average of the values relative to the two sides of the hybrid shell, one facing the DFP and the other in contact with water.

The vaporization point of the liquid DFP core of the DexMA nanodroplets, with an average diameter of 700 nm, is expected to shift at higher temperatures significantly in comparison to that of the microdroplets, having an average diameter of 4 μm, as a consequence of the larger Laplace pressure contribution. In fact, Figure 5 shows that the transition temperature of the DFP core of the nanodroplets is about 20 °C higher than that of microdroplets with same composition and structure of the hybrid shell.

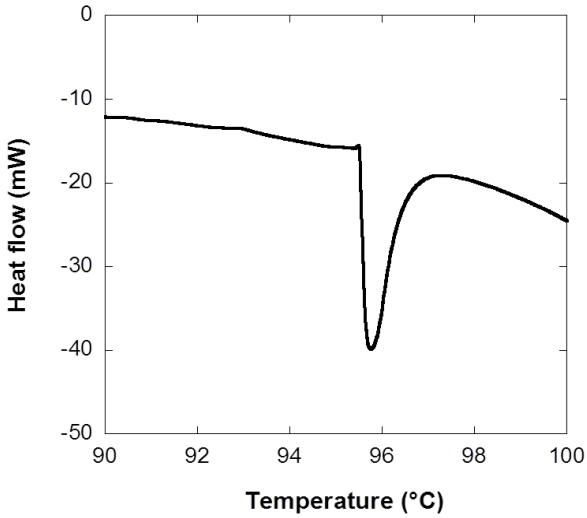

Figure 5. DSC thermogram of UV cured DexMA nanodroplets (average diameter of 700 nm). Exothermic heat: up.

It is worthy to note that the peak shown in Figure 5 recovers the simple profile of the thermogram of uncured microdroplet ones, which denotes the low size polydispersity of the nanodroplets. The interfacial tensions for micro and nanodroplets with the same composition of the shell obtained from DSC measurements are reported in Table 1, together with the values measured with the pendant drop method.

Table 1. Summary of the interfacial tension values of UV cured droplets obtained by DSC and pendant drop methods.

Microdroplets interfacial tension from DSC* [$mN \cdot m^{-1}$]	Nanodroplets interfacial tension from DSC [$mN \cdot m^{-1}$]	Microdroplets interfacial tension from pendant drop method [$mN \cdot m^{-1}$]
37 ± 9	33 ± 5	26.1 ± 0.7

*the average value of 75 °C was used as transition temperature. Standard deviations were evaluated on three independent measurements

The interfacial tension values (first two column of Table 1) obtained by DSC for micro- and nanodroplets are in agreement within the experimental uncertainties. This corroborates the method, since the surface tension should depend only on the nature of the droplet shell, but not on the particle curvature. As expected, these values are higher than the interfacial tension ones obtained by using the pendant drop method, where the mixture was exposed to a shorter time of curing, presumably introducing a lower crosslinking degree of the polymer.

For amphiphilic block copolymers, such as poly(ethylene oxide)-poly(propylene oxide)-poly(ethylene oxide), or amphiphilic dextrans used as stabilizing interfacial agents in O/W emulsions, have been reported surface tension values in the range of 50 to 30 $mN \cdot m^{-1}$.[41,42]

ADV provokes a "droplet – to – bubble" expansion, which has been monitored using ultra-fast camera.[43,] Starting from a size of 2 μm, the shell expands to a stable size of 10 μm after a damped oscillation transient. In the case of UV cured DexMA droplets, the ADV driven droplet ↔ bubble phase shift, is triggered by the application of US, followed by the recovery of the droplet state when US are switched off. To understand the behaviour of the hybrid shell during the ADV process and the return to the initial state, droplets with a liquid DFP core tagged with the solvatochromic dye nile red were monitored by confocal microscopy. Nile red is often used as probe of the polarity of the dispersing medium.[44] Typically, Nile red fluorescence is enhanced in apolar media and is almost completely quenched in water. This feature can be used to monitor the state of the core during ADV and DFP re-condensation. In fact, there is a significant increase of the size upon the US application (MBs appearing as smaller rings are those out of the equatorial plane) and the nile red fluorescence in the particles core appears dimmed due to the low density of the vapour phase. After 15 minutes from US switching off, the particles return to the equilibrium state with an intense, evenly distributed fluorescence in the core. This behaviour is a clear evidence for evaporation and re-

condensation of DFP, that after the condensation is still encapsulated in the droplets (see Figure 6).

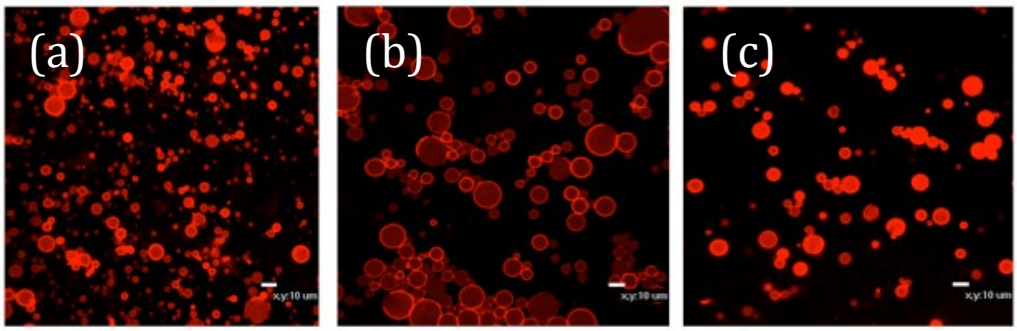

Figure 6. CLSM images of DexMA shelled MBs (no labelling of the shell) in the presence of Nile red in the DFP core. Before US irradiation, (a); 100 s after US irradiation, (b); after 15 min from US irradiation, (c).

The integrity of the droplets during the US "on-off" duty cycle is monitored by marking with RBITC (red fluorescence) the shells, while the aqueous medium surrounding the microbubbles is stained with FITC (green fluorescence). Confocal microscopy images were captured 100 s and 600 s after US switching off, (see figure 7). After 100 s from US switching off, i.e. while ADV is on-going, the shells of MBs are imaged as red contours surrounding black domains containing DFP in the gas state (Figure 7a). The green fluorescence is confined outside the shells and, most importantly, is absent in the internal domains, indicating that the shells are intact, without permeation of the outside medium into the core. After 600 s the bubbles returns to the pristine droplet state with a decrease of the average size (Figure 7b).

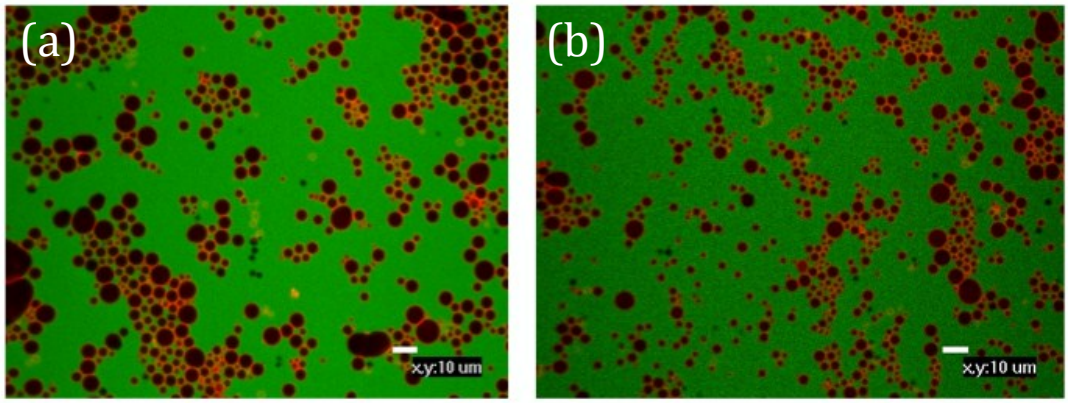

Figure 7. CLSM images of DexMA shelled MBs (red fluorescence) in the dispersing medium (green fluorescence) after 100 s, (a) and 600 s (b) from US excitation.

As counterproof, a sample of UV-uncured DexMA droplets, exposed to the same US dose and stained as for the sample showed in Figure 7, appears completely shattered, as highlighted in the CLSM image of Figure S5 of ESI. It can be concluded that the resistance of the shells to the US treatment is due to the UV curing of the DexMA shells.

Monitoring the shell dynamics after ADV

As compared with the ADV behaviour of lipid shelled MBs, our hybrid shell microdroplets undergo a 3-fold expansion, reaching the average size D_{US} of 9.6 μm. This value is comparatively lower than the 8-fold expansion to which decafluorobutane droplets dispersed in water are subjeted.[45] The core re-condensation down to the original droplet state after ADV can be regarded as a way to access the relaxation properties of the complex interface characterizing the novel hybrid lipid-polymer shelled MBs presented herein. As described in the experimental section, after US switching off, the size (diameter) reduction of individual MBs was monitored at varying time using CLSM (as an example, see Figure S6 of ESI). The results for 16 individual MBs are shown in Figure 8. It should be noted that the values of the MB diameters at t=0 are not shown in Figure 8 because a reliable measure of the size of the MB in the absence of the US field can be taken only when the residual turbulence in the surrounding liquid vanishes and this takes a few seconds.

Differently from pure lipid shells, after ADV, we could not find a single MB undergoing collapse, coalescence or steady oscillations, the radial shrinking was the only mechanism causing the return to the original microdroplet state. According to Figure 8, the original microdroplet state is reached only through radial shrinking. Moreover, the MB radial shrinking, accompanied by the condensation of the DFP vapour, is much slower than the US triggered expansion. These differences can be ascribed to the peculiar viscoelastic features of the lipid/crosslinked polymer shell.

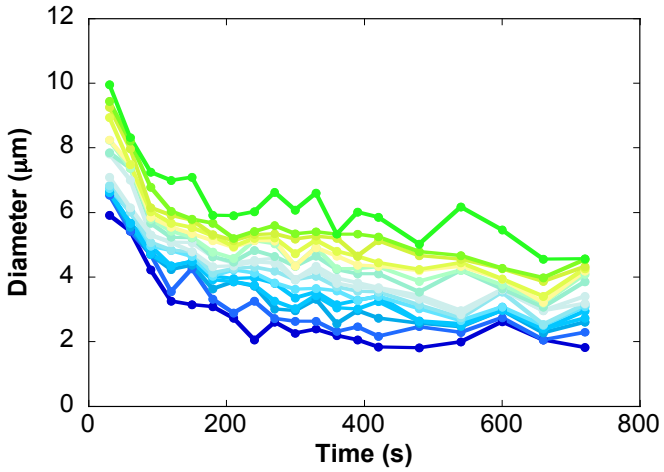

Figure 8. Time dependence of MB diameters. Time t=0 is chosen as the time at which US pressure field has been turned off. CLSM images could be captured only after 30 s from the end of the US irradiation.

By averaging the profiles shown in Figure 8, a master curve shown in Figure 9 is obtained, with error bars indicating the standard deviations of the size distribution at fixed times.

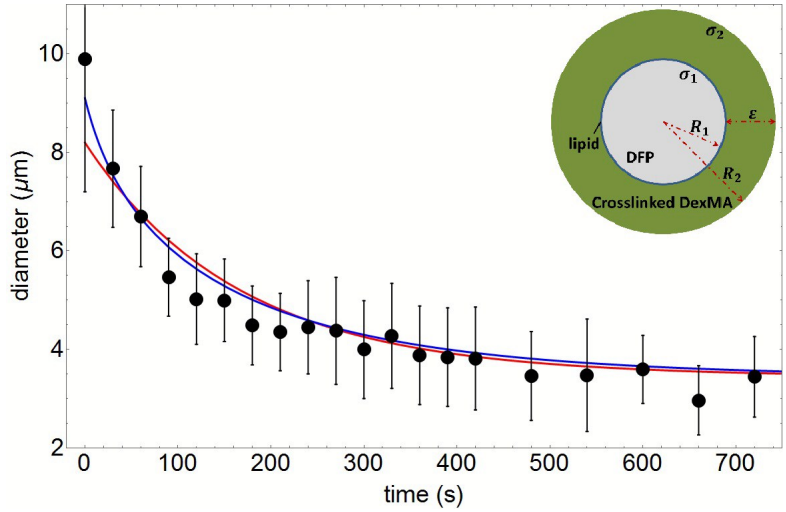

Figure 9. Dynamics of the average radial shrinking of polymer shelled MBs with DFP core, after ADV. At t=0, the average size D_{US} was imposed. The optimized solutions are shown for the MB wall modelled as a single thick shell (red line) and including the lipid shell confined at the DFP-polymer interface (blue line). Inset: description of the hybrid MB model showing the main parameters used in Church equation.

Radial shrinking simulation

MBs shells are generally composed of surfactants, lipids, synthetic or biological polymers, each one exhibiting different values of thickness and elasticity. The knowledge of both shell composition and thickness is fundamental to address appropriate model for simulating the relaxation process shown in Figure 9. The assembly of thick crosslinked polymer spherical surface, adjacent to a thin surfactant layers confined in the inner side of the polymer interface (see inset of Figure 9) results in a total shell thickness, ε, of ~ 300 nm, as measured by AFM on MBs collapsed in air (see Figure 10). The Church model provides the theoretical background to define the radial dynamics of thick polymer-shelled MBs with constant shear modulus G_S and viscosity μs.[46]

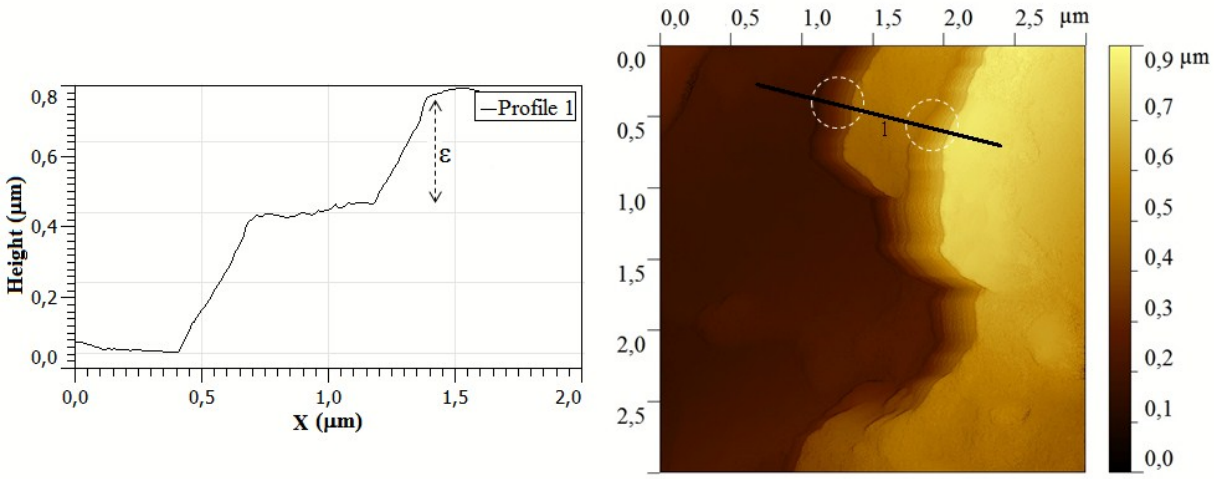

Figure 10. Left: AFM height profile for the evaluation of the shell thickness ε. Right: AFM micrograph of the edges (dashed circles) of a collapsed dry MB.

In this framework, we first treat the MB wall as a shell with a inner and outer interfaces σ_1 and σ_2, respectively, fixed to the experimental values σ_1 = 27.8 mN/m for the DFP/surfactant interfacial tension and $\sigma_2 - \sigma_1$ = 37 mN/m, where σ_2 indicates the water/polymer tension (see Table 1 of ESI). According to the Church's model, the bubble is described as a sphere, surrounded by an incompressible liquid of infinite extent. The liquid is assumed Newtonian, with a constant shear viscosity μ_L. The shell, defined by the internal and external radii R_1 and R_2, respectively, is described as an incompressible, viscoelastic material, with constant volume, V_s, shear viscosity, μ_s,

and shear modulus, G_s. These assumptions on the shell properties are particularly appropriate in our case as the relaxation of the microbubbles is a slow process ensuring the Newtonian behaviour of the hydrogel. To check our assumptions, we estimated the relaxation shear rate by the shell thickness relative variation $\Delta\varepsilon/\varepsilon$ per second, obtaining about 10^{-3} s^{-1}. We assumed this value low enough to frame the dynamics as Newtonian.[47] The density of the fully hydrated shell, ρ_S, is assumed similar to the shell density of MBs with a crosslinked PVA shell, previously determined, ensuring that the difference between the shell and water densities can be neglected in the model.[48, 49] It is important to consider that the microbubbles relaxation is accomplished after ADV, when the US field is off. In this condition, the DFP gas of the core condenses, remaining confined within the bubbles shell under critical conditions as the average value of the size of the bubbles at t=0 is below the critical volume of the DFP core.[50] Therefore the entire shrinking process occurs during the condensation at constant internal pressure, P_{IN}, and equal to a DFP vapour pressure of 34.2 kPa, calculated using the Antoine's law at a temperature of 300 K .[50]

The Church model is described by the equation:

$$R_1\ddot{R}_1 + \frac{3}{2}\dot{R}_1^2 = \frac{1}{\rho_S}\left[P_{IN} - P_0 - \frac{2\sigma_1}{R_1} - \frac{2\sigma_2}{R_2} - 4\frac{\dot{R}_1}{R_1}\left(\frac{V_S\mu_S + V_1\mu_L}{V_2}\right) - 4\frac{V_S G_S}{V_2}\left(1 - \frac{R_{1eq}}{R_1}\right)\right] \qquad (3)$$

where V_1 and V_2 are the core and the core-plus-shell volume of the MB, respectively, P_0 is the external pressure and ρ_S represents the density of water. The R_{1eq}, the relaxed equilibrium position of the internal interface, is obtained by setting $\dot{R}_1$ and $\ddot{R}_1$ equal to zero:[51]

$$R_{1eq} = R_{01}\left\{1 + \frac{4\pi R_{02}^3}{12 G_S V_S}\left[\left(\frac{2\sigma_1}{R_{01}} + \frac{2\sigma_2}{R_{02}}\right) - \left(P_{IN}^{eq} - P_0\right)\right]\right\} \qquad (4)$$

with P_{IN}^{eq}, R_{01} and R_{02} indicating the internal pressure and the radii of the two interfaces at equilibrium, respectively. The boundary condition of volume constancy of the shell during the process is expressed by:

$$R_2 = R_1\sqrt[3]{1 + \frac{V_S}{V_1}} \qquad (5)$$

The numerical solution of the Church equation is optimized in order to obtain the fit shown in Figure 9, red line. The model, eq 3, describes well the shrinking process of the elastomeric shell. To further validate the model used in this analysis, the average MB diameter at t=0, D_0, was treated as an independent fitting parameter and compared with the average experimental value, D_{US}, (Figure S6 of ESI).

In order to treat the relaxation of the hybrid shell made of surfactant and crosslinked polymer layers, the Church dynamic equation is implemented according to the Marmottant's model.[52, 53] We introduce an elastic tension, κ, which describes the behaviour of the surfactant layer confined at the polymer-DFP interface.[53] This is obtained by substituting the internal surface tension, σ_1, of the Church model, eq 4, with the sum of the equilibrium value, i.e. 27.8 mN/m reported in Table 1 of ESI, and of a restoring stiffness, σ_L, which depends on the stretched surface of the surfactant layer, accoding to eq 6.

$$\sigma_L(R_1) = \kappa \frac{\Delta A}{A_{eq}} = \kappa \frac{4\pi R_1^2 - A_{eq}}{A_{eq}} \qquad (6)$$

where A_{eq} is the area of the non-stretched lipid wall, known from the internal radius at the end of the relaxation dynamics. Treatment of σ_L as a free parameter in the model, it allows to uncouple the stiffness value of the surfactant layer forced on the MB shell from the polymer layer contribution. Interestingly, the fit of this model (Figure 9, blue line) provides a reduced χ^2 comparatively lower, i.e. from a value of 3.2 it decreases to 1.8, as reported in Table 2. The obtained value of lipid elastic tension, κ, is in line with the values found for other surfactant shelled MBs, as SonoVue®.[52] Moreover, the values of σ_1 and σ_2, treated as free parameters, are more stable in the latter case and closer to the corresponding experimental values. The fitting parameters obtained by the numerical integration from both the Church and the Church-modified models, red and blue lines in Figure 9, respectively, are summarized in Table 2. As derived from the χ^2 analysis, the description is improved when it includes the elastic modulus of the surfactant monolayer of the shell (compare 2nd and 3rd columns of Table 2).

Table 2. Viscoelastic parameters of the optimized numerical solution of eq. 3. Errors are estimated from the χ^2 minimization.

Best-fit parameters	**Church model** ($\chi^2 = 3.2$)	**Hybrid shell model** ($\chi^2 = 1.8$)
G_S (MPa)	6.3±0.2	3.9±0.2
μ_S (GPa·s)	1.22±0.03	1.02±0.03
D_0 (μm)	8.2±0.1	9.1±0.1
κ (mN/m)	—	130±5

The shear modulus, G_S, is consistent with the values typical of other polymer shelled MBs, such as Quantison®, Albunex®, Optison®. [51, 54] The striking feature exhibited by these crosslinked polymer shelled MBs is the long lasting radial shrinking process with a relaxation time of a few hundreds of seconds and it can be explained in the light of the very high shear viscosity of the shell, μ_s, around 1 GPa. This value is orders of magnitude larger than the viscosities of other MBs polymer shells reported in literature.[55] This difference can be reasonably attributed to the comparatively large difference of the frequency of deformation at which our system and those previously reported were subjected.[56] In fact, differently from our case, shell viscosity of the MB was usually estimated by solving the Church's model in the presence of a forcing ultrasonic field, a condition that imposes a high rate of shell deformation. Indeed, for high rate of oscillation the viscosity of a same MB shell is expected to be strongly reduced.[57] Moreover, the shell-induced damping of the oscillation becomes more pronounced when the shell thickness increases.[58] On the contrary, due to the slow rate of radial relaxation of our hybrid MBs, it would be more suitable to compare the viscosity of the corresponding bulk polymer network, at very low shear rates. Preliminary bulk viscosity measurements performed on crosslinked DexMA, the polymer network of the MB shell, provides a value of 0.1 MPa·s at a shear rate of ~10^{-3} s^{-1}, evidencing that the highly viscous contribution of the MB radial dynamics estimated herein is mainly dictated by the thick polymer part of the hybrid MB shell. Simulations pointed out that the lowest viscosity range capable to reproduce the experimental

time scale is of the order of 10^8 Pa·s. Only values of such a magnitude allow matching the simulated dynamics with experimental time window (see Figure S7 of ESI). However, this does not impede a good scattering ability with a super harmonic response displayed by the MBs as determined by a previous study on the US behaviour of these MBs.[11] One result of this study highlights that the peak negative pressure threshold values necessary to transform our microdroplets into an UCA, are compatible with the safety limits suggested by medical directories. Several reports point out that the viscosity (as well as the Young modulus) of strongly confined materials with high curvature and nanometric thickness may differ, often increasing, by several orders of magnitude from the corresponding bulk one at macroscopic length scale.[56] The viscosity herein evaluated seems dramatically dictated by the hollow-shell confinement geometry of the employed polymer. The development of a host of scanning surface probe tools enables experimentalist to monitor within molecular dimensions the rheological behaviour of soft condensed matter interfaced with substrates. However, under condition of severe confinement, a direct study of the relation between the material properties and the microscopic structure of confined phases still remains an experimental challenge. In this respect, we show here a way to access detailed information on viscoelastic properties of the MB shell, otherwise difficult to achieve.

CONCLUSIONS

The encapsulation of DFP by a hybrid shell made of two surfactants, i.e. Epikuron®200 and PA, and a biodegradable polymer network can be accomplished in micron- and nano- sized droplets. This study focuses on the new properties of these droplets with complex shells. The polymer deposition on the surfactants layer is based on the amphiphilic character of methacryloyl-grafted dextran chains, which are able to assemble on the surfactant shell encapsulating the hydrophobic DFP liquid core. The photopolymerization of the vinyl moiety brought by the dextran chains introduces the crosslinks, which transform a polymer layer into a permanent viscoelastic membrane contrasting coalescence and providing repeatability to stress/deformation process. With a boiling point of 56 °C, DFP cannot be described as an overheated liquid at physiological conditions. Moreover, the Laplace pressure imposed by the spherical shell has the effect to additionally increase the boiling point of the encapsulated DFP. However, ADV, the droplet ↔ microbubbles transition, can be accomplished by exposing the droplets in a static modality to US typically used for sonoporation with an MI of 0.3, well below the safety limitations requested for medical use. The polymer network behaves as a viscoelastic membrane when ADV is triggered by US with a three-fold increase the diameter. After switching off the US pressure field, the gaseous core of the MBs condenses, as the molar volume of the encapsulated DFP is smaller than its critical volume. The shell complies with the gas condensation recovering the initial droplet dimensions with a characteristic relaxation time, linked to the viscoelastic properties of the shell. A CLSM analysis of the time evolution of the diameters allows accessing the micro-rheology behaviour of the hybrid shell by modifying available models describing the MBs dynamics. These “phase-shift” systems can support both the transport of hydrophobic drugs dissolved in the DFP liquid core and US imaging after the transition to MBs by the action of the same probe used for the sonographic detection.

Notes

The Authors declare no competing financial interests.

ACKNOWLEDGEMENT

This work was supported by the European Union Seventh Framework Programme FP7/2007-2013 under grant agreement n. 602923 "TheraGlio" and by INAIL, the grant agreement n. 7290 BRIC 2015. The assistance of Dr. Susanna Laurén of Biolin Scientific, Finland, for interfacial tension measurements and of Dr. Nadia Decarolis for the organization of the visit of SC to Biolin Scientific is acknowledged with thanks. We thank Mr. R. Palomba and Dr. C. Giliberti of INAIL for helpful discussions.

REFERENCES

1 S. Qin, C. F. Caskey, and K. W. Ferrara, *Phys. Med. Biol*., 2009, **54**, R27.

2 S. B. Feinstein, *Am. J. Physiol.*, 2004, **287**, H450.

3 J. R. Lindner, *Nat. Rev. Drug Discov.*, 2004, **3**, 527.

4 A. Günther and K. F. Jensen, *Lab Chip*, 2006, **6**, 1487.

5 P. Marmottant, J. P. Raven, H. Gardeniers, J. G. Bomer and S. Hilgenfeldt, *J. Fluid. Mech.*, 2006, **568**, 109.

6 M. Abolhasani, A. Oskooei, A. Klinkova, E. Kumacheva and A. Günther, *Lab Chip*, 2014, **14**, 2309.

7 O. Gunduz, Z. Ahmad, E. Stride, and M. A. Edirisinghe, *Mater. Sci. Eng. C Mater. Biol. Appl.*, 2012, **32**, 1005.

8 E. Talu, M. M. Lozano, P. A. Dayton and M. Longo, *Langmuir*, 2006**, 22**, 9487.

9 M. R. Böhmer, R. Schroeders, J. A. M. Steenbakkers, S. H. P. M. D. Winter, P. A. Duineveld, J. Lub, W. P. M. Nijssen, J. A. Pikkemaat and H. R. Stapert, *Colloids Surf., A Physicochem. Eng. Asp*., 2006, **289**, 96.

10 B. J. Schmidt, I. Sousa, A. A. van Beek and M. R. Böhmer, *J. Control. Release*, 2008, **131**, 19.

11 S. Capece, E. Chiessi, R. Cavalli, P. Giustetto, D. Grishenkov and G. Paradossi, *Chem. Commun*., 2013, **49,** 5763.

12 E. G. Schutt, D. H. Klein, R. M. Mattrey and J. G. Riess, *Angew. Chem. Int. Ed.*, 2003, **42,** 3218.

13 H. Dewitte, B. Geers, S Liang, U. Himmelreich, J. Demeester, S. C. De Smedt and I. Lentacker, *J. Control. Release*, 2013, **169**, 141.

14 S. Sirsi and M. Borden, *Bubble Sci. Eng. Technol.*, 2009, **1**, 3.

15 D. Grishenkov, L. Kari, L. Å. Brodin, T. B. Brismar and G. Paradossi, *Ultrasonics*, 2011, **51**, 40.

16 V. Sanna, G. Pintus, P. Bandiera, R. Anedda, S. Punzoni, B. Sanna, V. Migaleddu, S. Uzzau and M. Sechi, *Mol. Pharmaceutics*, 2011, **8**, 748.

17 X. Xiong, F. Zhao, M. Shi, H. Yang and Y. Liu, *J. Biomater. Sci. Polym. Ed*., 2011, **22**, 417.

18 P. S. Sheeran and P. A. Dayton, *Scientifica*, 2014, DOI: 10.1155/2014/579684.

19 O. D. Kripfgans, M. L. Fabiilli, P. L. Carson, J. B. Fowlkes, *J. Acoust. Soc. Am.*, 2004, **116**, 272.

20 P. S. Sheeran, S. Louis, P. A. Dayton and T. O. Matsunaga, *Langmuir*, 2011, **27**, 10412.

21 O. D. Kripfgans, J. B. Fowlkes, D. L. Miller, O. P. Eldevik and P. L Carson, *in Med. and Biol.*, 2000, **26**, 1177.

22 N. Rapoport, *Rev. Nanomed. Nanobiotechnol.*, 2012, **4**, 492.

23 S. Hernot and A. L. Klibanov, *Adv. Drug Deliv. Rev.*, 2008, **60**, 1153.

24 R. Suzuki, T. Takizawa, Y. Negishi, K. Hagisawa, K. Tanaka, K. Sawamura, N. Utoguchi, T. Nishioka and K. Maruyama, *J Control. Release*, 2007, **117**, 130.

25 G. A. Husseini, G. D. Myrup, W. G. Pitt, D. A. Christensen and N. Y. Rapoport, *J. Control. Release*, 2000, **69**, 43.

26 E. Rotureau, M. Leonard, E. Dellacherie and A. Durand, *J. Colloid Interface Sci.*, 2004, **279**, 68.

27 S. Mehier-Humbert, F. Yan, P. Frinking, M. Schneider, R. H. Guy and T. Bettinger, *Bioconjug. Chem.,* 2007, **18**, 652.

28 M. L. Fabiilli, K. J. Hawoeth, I. E. Sebastian, O. D. Kripfangs, P. L. Carson and J. B. Fowlkes, *Ultrasound Med. Biol.*, 2010, **36**, 1364.

29 P. A. Mountford, A. N. Thomas and M. A. Borden, *Langmuir*, 2015, **31**, 4627.

30 P. A. Mountford, S. R. Sirsi and M. A. Borden, *Langmuir*, 2014, **30**, 6209.

31 O. D. Kripfgans, J. B. Fowlkes, D. L. Miller, O. Petter Eldevik, P.L. Carson, *Ultrasound in Med. & Biol.,* 2000, **7**, 1177.

32 N. Y. Rapoport, A. M. Kennedy, J. E. Shea, C. L. Scaife and K.-H. Nam, *J. Control. Release*, 2009, **138**, 268.

33 O. Shpak, M. Verweij, H. J. Vos, N. de Jong, D. Lohse and M. Versluis, *Proc. Nat. Acad. Sci. U.S.A.*, 2014, **111**, 1697.

34 F. Domenici, C. Giliberti, A. Bedini, R. Palomba, I. Udroiu, L. Di Giambattista, D. Pozzi, S. Morrone, F. Bordi and A. Congiu Castellano, *Ultrasonics*, 2014, **54**, 1020.

35 E. Rotureau, M. Leonard, E. Dellacherie and A. Durand, *Phys. Chem. Chem. Phys.*, 2004, **6**, 1430.

36 G. L. Fang, L. Cao and F. Shan, *Mater. Chem. Phys.*, 2012, **137**, 558.

37 M. C. Bautista, O. Bomati-Miguel, M. del Puerto Morales, C. J. Serna and S.Venteimillas-Vardaguer, *J. Magn. Magn. Mater.*, 2005, **293**, 20.

38 H. Bunjes, M. H. Koch and K. Westesen, *Langmuir*, 2000, **16**, 5234.

39 B. Strasdat and H. Bunjes, *Food Hydrocoll.*, 2013, **30**, 567.

40 P. Evans, D. P. Parson and V. S. J. Craig, *Langmuir*, 2006, **22**, 9538.

41 P. Alexandridis and T. A. Hatton, *Colloids Surf. A Physicochem. Eng. Asp.*, 1995, **96**, 1.

42 P. Imbert, V. M. Sadtler and E. Dellacherie, *Colloids Surf A: Physicochem. Eng. Asp.*, 2002, **211**, 157.

43 N. Reznik, O. Shpak, E. C. Gelderblom, R. Williams, N. de Jong, M. Versluis and P. N. Burns, *Ultrasonics*, 2013, **53**, 1368.

44 P. Greenspan, E. P. Mayer, S. D. Fowler, *J. Cell Biol.*, 1985, **100**, 965.

45 P. S. Sheeran, T. O. Matsunaga and P. A. Dayton, *Phys. Med. Biol*., 2014, **59**, 379.

46 C. C. Church, *J. Acoust. Soc. Am.*, 1995, **97**, 1510.

47 R. K. Gupta, *Polymer and Composite Rheology*, CRC Press, Boca Raton, 2000.

48 F. Cavalieri, A. El Hamassi, E. Chiessi and G. Paradossi, *Langmuir*, 2005, **21**, 8758.

49 P. A. L. Fernandez, G. Tzvetkov, R. H. Fink, G. Paradossi and A. Fery, *Langmuir*, 2008, **24**, 13677.

50 K. Tochigi, C. Kikugi, K. Kurihara, K. Ochi, J. Mizukado and K. Otake, *J. Chem. Eng. Data*, 2005, **50**, 784.

51 D. B. Khismatullina, *J. Acoust. Soc. Am.*, 2004, **116**, 1463.

52 P. Marmottant, S. van der Meer, M. Emmer, M. Versluis, N. de Jong, S. Hilgenfeldt and D. Lohse, *J. Acoust. Soc. Am.,* 2005**, 118**, 3499.

53 N. de Jong, M. Emmer, A. van Warmel and M. Versluis, *Med. Biol. Eng. Comput*., 2009, **47**, 861.

54 F. Domenici, F. Dell'Unto, D. Triggiani, C. Olmati, C. Castellano, F. Bordi, A. Tiezzi and A Congiu, *Biochim. Biophys. Acta*, 2015, **1850**, 759.

55 D. A Chatterjee, *Ultrasound in Med. & Biol.*, 2003, **29**, 1749.

56 D. Grishenkov, C. Pecorari, T. B. Brismar and G. Paradossi, *Ultrasound in Med. and Biol.*, 2009, **35**, 1139.

57 M. Schoen, in *Computational Methods in Surface and Colloids Science*, ed. M. Borówko, CRC Press: Boca Raton, 2000, chapter 1, pp. 3-11.

58 J. Paulose, G. A. Vliegenthart, G. Gompper and D. R. Nelson, *Proc. Natl. Acad. Sci. U.S.A.*, 2012, **109**, 19551.

59 F. K. Oppong and J. R. de Bruyn, *J. Non-Newtonian Fluid Mech.*, 2007, **142**, 104.

Graphical abstract